

---

---

**REPORT 1187**

---

**THEORETICAL AND EXPERIMENTAL INVESTIGATION  
OF ADDITIVE DRAG**

**By MERWIN SIBULKIN**

**Lewis Flight Propulsion Laboratory  
Cleveland, Ohio**

---

---

# National Advisory Committee for Aeronautics

*Headquarters, 1512 H Street NW., Washington 25, D. C.*

Created by act of Congress approved March 3, 1915, for the supervision and direction of the scientific study of the problems of flight (U. S. Code, title 50, sec. 151). Its membership was increased from 12 to 15 by act approved March 2, 1929, and to 17 by act approved May 25, 1948. The members are appointed by the President, and serve as such without compensation.

JEROME C. HUNSAKER, Sc. D., Massachusetts Institute of Technology, *Chairman*

DETLEV W. BRONK, Ph. D., President, Rockefeller Institute for Medical Research, *Vice Chairman*

JOSEPH P. ADAMS, LL. D., member Civil Aeronautics Board.  
ALLEN V. ASTIN, Ph. D., Director, National Bureau of Standards.  
PRESTON R. BASSETT, M. A., President, Sperry Gyroscope Co., Inc.  
LEONARD CARMICHAEL, Ph. D., Secretary, Smithsonian Institution.  
RALPH S. DAMON, D. Eng., President, Trans World Airlines, Inc.  
JAMES H. DOOLITTLE, Sc. D., Vice President, Shell Oil Co.  
LLOYD HARRISON, Rear Admiral, United States Navy, Deputy and Assistant Chief of the Bureau of Aeronautics.  
RONALD M. HAZEN, B. S., Director of Engineering, Allison Division, General Motors Corp.

RALPH A. OFSTIE, Vice Admiral, United States Navy, Deputy Chief of Naval Operations (Air).  
DONALD L. PUTT, Lieutenant General, United States Air Force, Deputy Chief of Staff (Development).  
DONALD A. QUARLES, D. Eng., Assistant Secretary of Defense (Research and Development).  
ARTHUR E. RAYMOND, Sc. D., Vice President—Engineering, Douglas Aircraft Co., Inc.  
FRANCIS W. REICHELDERFER, Sc. D., Chief, United States Weather Bureau.  
OSWALD RYAN, LL. D., member, Civil Aeronautics Board.  
NATHAN F. TWINING, General, United States Air Force, Chief of Staff.

---

HUGH L. DRYDEN, Ph. D., *Director*

JOHN F. VICTORY, LL. D., *Executive Secretary*

JOHN W. CROWLEY, JR., B. S., *Associate Director for Research*

EDWARD H. CHAMBERLIN, *Executive Officer*

---

HENRY J. E. REID, D. Eng., Director, Langley Aeronautical Laboratory, Langley Field, Va.

SMITH J. DEFRANCE, D. Eng., Director, Ames Aeronautical Laboratory, Moffett Field, Calif.

EDWARD R. SHARP, Sc. D., Director, Lewis Flight Propulsion Laboratory, Cleveland Airport, Cleveland, Ohio

---

LANGLEY AERONAUTICAL LABORATORY  
Langley Field, Va.

AMES AERONAUTICAL LABORATORY  
Moffett Field, Calif.

LEWIS FLIGHT PROPULSION LABORATORY  
Cleveland Airport, Cleveland, Ohio

*Conduct, under unified control, for all agencies, of scientific research on the fundamental problems of flight*

# REPORT 1187

## THEORETICAL AND EXPERIMENTAL INVESTIGATION OF ADDITIVE DRAG <sup>1</sup>

By MERWIN SIBULKIN

### SUMMARY

The significance of additive drag is discussed and equations for determining its approximate value are derived for annular- and open-nose inlets. Charts are presented giving values of additive drag coefficient over a range of free-stream Mach numbers for open- and for annular-nose inlets with conical flow at the inlet. The effects on additive drag of variable inlet-total-pressure recovery and static pressures on the centerbody are investigated and an analytical method of predicting the variation of pressure on the centerbody with mass-flow ratio is given.

Experimental additive-drag values are presented for a series of 20° and 25° cone half-angle inlets and one open-nose inlet operating at free-stream Mach numbers of 1.8 and 1.6. A comparison with the theoretical values of additive drag shows excellent agreement for the open-nose inlet and moderately good agreement for the annular inlets.

### INTRODUCTION

In the analysis of engine performance, it has been customary to define a net-thrust term that is evaluated between the outlet of the engine and a station ahead of the engine where the entering stream tube is at free-stream conditions. If the area of the entering stream tube at free-stream conditions is not equal to the inlet area, conditions at the inlet differ from those in the free stream; and if the flight velocity is supersonic, an additional force must be considered in determining the net propulsive thrust. This additional force has been called additive drag (ref. 1). The additive drag encountered at subsonic speeds is included in the analysis of reference 2.

A theoretical method of predicting the magnitude of the additive drag at supersonic speeds that is based upon an analysis of the location of detached shock waves as a function of relative mass flow and Mach number is included in reference 3. Dailey and McFarland of the University of Southern California in 1950 suggested a method of computation based upon an analysis of the entering stream tube. Suggested by Nucci of the NACA Langley laboratory in 1950 was a method which makes use of the external shock configuration. For configurations having side inlets, an analysis of the effect of changes in the entering air conditions ahead of the inlet is given in reference 4.

In this report, prepared at the Lewis laboratory in 1950, the necessity for including the effect of additive drag in calculating the net propulsive thrust is discussed and a

modified method of predicting the additive drag based on an analysis of the entering stream tube is presented. Theoretical values calculated by the modified method are compared with the values predicted by the methods of Dailey and of reference 3. Comparison is also made with experimental values of additive drag obtained from tests of ram-jet models in the Lewis 8- by 6-foot supersonic tunnel. Also included in this report is a comparison of experimental additive drag values with those predicted by the external shock method.

### SYMBOLS

The following symbols are used in this report:

$A$	flow area, sq ft
$A_c$	capture area, cross-sectional area at cowl lip including centerbody area, sq ft
$A_s$	cross-sectional area of centerbody at station 1, sq ft
$A_x$	component of surface area perpendicular to longitudinal axis of inlet, sq ft
$A_y$	area of centerbody where it is intersected by bow wave, sq ft
$C_{d,a}$	additive-drag coefficient, $2D_a/\rho_0 V_0^2 A_c$
$C_{f,s}$	friction-force coefficient on center body, $2F_{f,s}/\rho_0 V_0^2 A_c$
$C_s$	incremental-cone-pressure coefficient, $2A_s(\bar{p}_s - p_c)/\rho_0 V_0^2 A$
$D_a$	additive drag, lb
$F$	total momentum, $mV + A(p - p_0)$ , lb
$F_d$	sum of external pressure and friction drags, lb
$F_{f,s}$	axial component of force on fluid due to friction on portion of centerbody forward of station 1, lb
$F_j$	jet thrust, $mV_e + A_e(p_e - p_0)$ , lb
$F_n$	net thrust, lb
$F_{n,t}$	net internal thrust, lb
$F_p$	inertial reaction of net propulsive thrust, lb
$F_s$	scoop incremental drag, lb
$g$	acceleration due to gravity, ft/sec <sup>2</sup>
$K$	bow-wave-position parameter
$M$	Mach number
$m$	mass-flow rate of fluid passing through inlet, slugs/sec
$m_{max}$	maximum theoretical rate of mass flow through capture area $\equiv \rho_0 V_0 A_c$ , slugs/sec
$P$	total pressure, lb/sq ft abs
$p$	static pressure, lb/sq ft abs
$p_c$	theoretical static pressure on surface of cone behind an oblique shock, lb/sq ft abs
$\bar{p}_s$	effective static pressure on portion of centerbody forward of station 1, lb/sq ft abs

<sup>1</sup>Supersedes NACA RM E51B13, "Theoretical and Experimental Investigation of Additive Drag" by Merwin Sibulkin, 1951.

$p_w$	theoretical static pressure immediately behind an oblique shock wave, lb/sq ft abs
$R$	gas constant, ft <sup>3</sup> /°R
$T$	total temperature, °R
$V$	velocity, ft/sec
$\beta$	ratio of mass-flow rate with supersonic flow at inlet to maximum theoretical capture-area mass flow
$\gamma$	ratio of specific heats
$\theta_c$	cone half-angle of inlet centerbody
$\theta_i$	cowl-position parameter, angle between axis of inlet and straight line that connects tip of centerbody lip of cowl
$\lambda$	angle at station 1 between average direction of flow and longitudinal axis of inlet
$\rho$	density, slugs/cu ft
Subscripts:	
0	free stream
1	conditions at engine inlet (defined in text for particular types of inlet)
$e$	conditions at engine outlet

### ANALYSIS

The net propulsive thrust of an engine at zero angle of attack is the resultant of the sum of the axial components of the pressure and friction forces acting on the engine. A schematic representation of these forces as applied to a ram-jet engine in accelerated flight is shown in figure 1, in which the net propulsive thrust of the engine is replaced by an equal

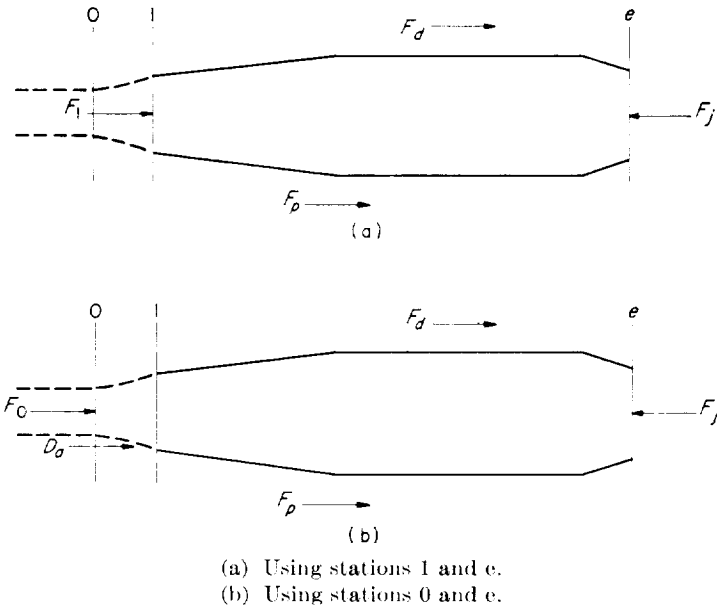


FIGURE 1.—Schematic representation of forces acting on ram-jet engine in accelerated flight.

and opposite inertial force  $F_p$  according to D'Alembert's principle for accelerating systems. The forces are defined as positive in the directions shown by the arrows.

The sum of pressure and friction forces acting on the interior of the engine, which is called the net internal thrust  $F_{n,i}$ , can be calculated from the change in total momentum  $mV + A(p - p_0)$  between stations 1 and  $e$  of the fluid passing through the engine (fig. 1(a)), that is,

$$F_{n,i} = F_j - F_1 \quad (1)$$

where  $F_j \equiv mV_e + A_e(p_e - p_0)$  and  $F_1 \equiv mV_1 + A_1(p_1 - p_0)$ .

Then

$$F_p = F_{n,i} - F_d \quad (2)$$

where  $F_d$  is the sum of the pressure and friction forces acting on the exterior of the engine.

It is customary, however, to evaluate engine performance between stations 0 and  $e$  (fig. 1(b)) and to call the change in total momentum of the internal flow (between stations 0 and  $e$ ) the net thrust  $F_n$  as given by

$$F_n = F_j - F_0 \quad (3)$$

where

$$F_0 \equiv mV_0 + A_0(p_0 - p_0) = mV_0$$

In this case, however,

$$F_p \neq F_n - F_d$$

because the change in total momentum of the free stream between stations 0 and 1 has not been considered. Therefore, in order to obtain the net propulsive thrust  $F_p$ , this momentum change (which is called additive drag  $D_a$ ) must be included to give

$$F_p = F_n - F_d - D_a \quad (4)$$

A mathematical definition of additive drag can be obtained by combining equations (1) to (4) to give

$$D_a = F_n - F_{n,i} = F_1 - F_0 \quad (5)$$

or using the definitions of  $F_1$  and  $F_0$ ,

$$D_a = mV_1 + A_1(p_1 - p_0) - mV_0 \quad (5a)$$

where appropriate average values of the quantities at station 1 are used.

Another interpretation (which gives physical meaning to net thrust  $F_n$ ) is to consider that the diverging portion of the entering stream tube behind a bow wave (fig. 2(a)) from I to II is replaced by a thin, frictionless membrane (fig. 2(b)). Inasmuch as the flow field is unchanged, the net propulsive thrust  $F_p$  will not be affected. Because the engine has

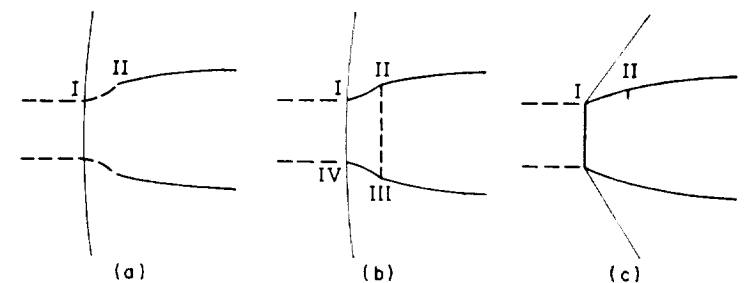


FIGURE 2.—Schematic representation of additive-drag elimination by cowl extension.

already been credited with the thrust due to the pressure acting on the interior of the hypothetical extension of the engine from I to II by its inclusion in the net thrust  $F_n$ , a drag force must be added because of the pressure acting on the exterior of the engine extension which is equal to

$$\int_I^{II} (p - p_0) dA_x$$

where  $dA_x$  is the axial projection of the surface area. This integral may also be used to define the additive drag and is equivalent to the definition given by equation (5a), as can easily be seen by applying the momentum theorem around the surface I, II, III, IV, I in figure 2 (b).

Although no change in the forces on the inlet occurs when an inlet is extended to free-stream diameter along a streamline, an increase in net propulsive thrust would be obtained if the inlet were extended in the manner shown in figure 2 (c). In this case the angle through which the entering streamline is turned is made smaller than the detachment angle and the bow wave is replaced by a normal shock at the entrance to the inlet and an oblique shock off the lip. Comparison of the modified inlet in figure 2 (c) with the one in figure 2 (a), shows that the increase in the cowl-pressure drag owing to the extension of the inlet from II to I is much less than the value of the additive drag eliminated because the increase in pressure behind the oblique shock in figure 2 (c) is much less than the pressure rise behind the nearly normal shock in figure 2 (a).

Equation (5a) applies directly only to an open-nose inlet. The comparable equation for an annular-nose inlet can be derived by considering the forces acting on the surface bounded by I, II, III, IV, V, I as shown in figure 3 (a). A summation of the axial components of the forces acting on the enclosed fluid gives

$$D_a = mV_1 \cos \lambda + A_1 \cos \lambda (p_1 - p_0) + A_s (\bar{p}_s - p_0) - mV_0 + F_{f,s} \quad (5b)$$

where  $A_1$  corresponds to the flow area II, III, and  $A_s(\bar{p}_s - p_0)$  and  $F_{f,s}$  are, respectively, the axial components of the pressure and the friction forces acting on the centerbody, and appropriate average values are used at station 1 and on the centerbody. Again, as in the case of the open-nose inlet, a definition of additive drag equivalent to equation (5b) is

$$D_a = \int_I^{II} (p - p_0) dA_x$$

A side- or scoop-type inlet can be considered to be an annular-nose inlet with the centerbody greatly extended (fig. 3 (b)) and, consequently, its additive drag can be found from equation (5b).

If, however, the scoop does not extend completely around the centerbody, it is extremely difficult to determine the portion of the centerbody which forms part of the boundary of the entering stream tube (indicated by shaded surface on diagram) and, consequently, to determine the proper value of  $A_s$  for use in equation (5b). Furthermore, for this type of fuselage, the drag on the shaded portion of the centerbody is customarily included in the body drag. Conse-

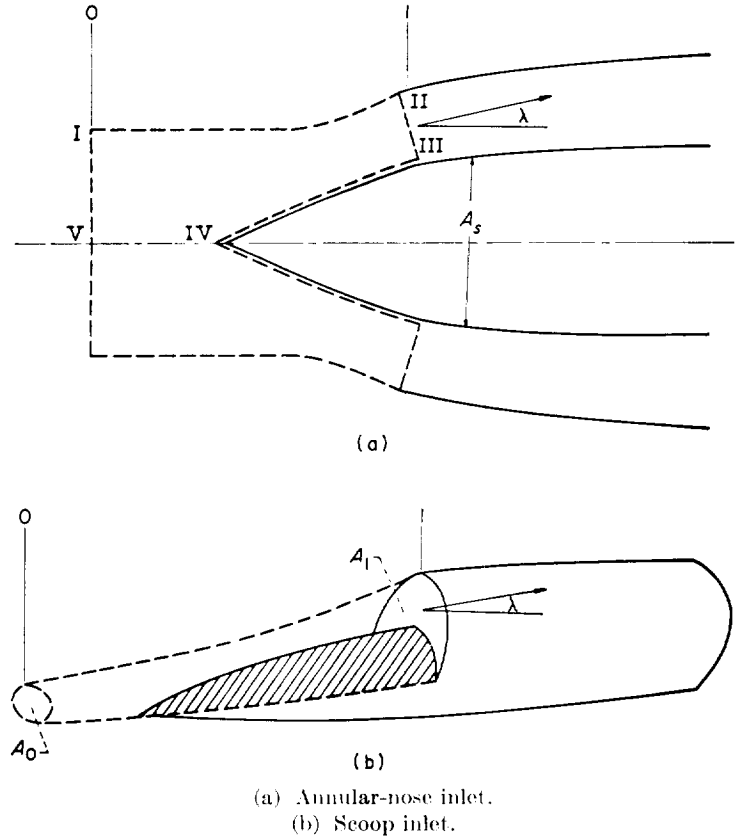


FIGURE 3.—Schematic views of annular-nose- and scoop-type inlets.

quently, reference 4 suggests that, if the approximation is made that the drag on the shaded portion of the centerbody does not change as the mass flow through the engine changes, then a scoop incremental drag  $F'_s$  can be defined equal to the change in total momentum of the entering stream tube between station 0 and 1; that is,

$$F'_s = mV_1 \cos \lambda + A_1(p_1 - p_0) - mV_0 \quad (5c)$$

Then

$$F'_p = F_n - F'_a - F'_s$$

where  $F'_a$  includes the drag on the shaded portion of the centerbody. If the direction of flow at station 1 is parallel to the axis, the formulas for evaluating the scoop incremental drag and the additive drag of an open-nose inlet (eq. (5a)) are the same.

#### APPARATUS AND PROCEDURE

Experimental values of additive drag were obtained in the NACA Lewis 8- by 6-foot supersonic tunnel for one open-nose and several annular-nose inlets. The inlets formed the forward end of a 16-inch ram-jet configuration, which is schematically shown in figure 4. Two cone angles were tested; the projection of the centerbodies was varied by cylindrical spacer blocks so as to obtain various supercritical mass-flow ratios. The values of cone angle, centerbody position, and design mass-flow ratio investigated are given in the table appearing in figure 4.

Tests were conducted at free-stream Mach numbers of 1.8 and 1.6 over a range of mass-flow ratio, which was controlled by a variable-area orifice valve located in the engine

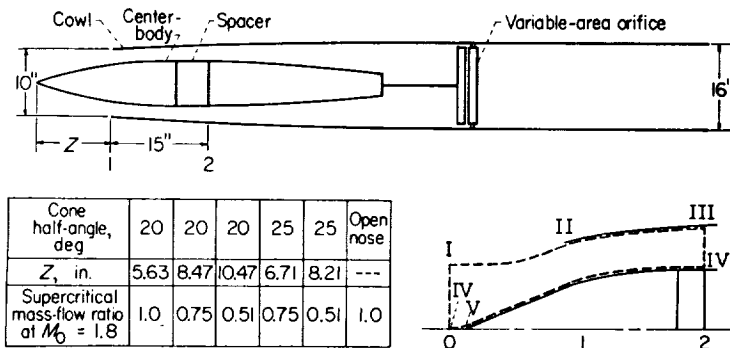


FIGURE 4.—Schematic diagram of inlet configurations investigated.

combustion chamber. Static pressures on the internal surface of the cowl and on the centerbody forward of station 2 (located 15 in. back of cowl lip) were measured by wall orifices, and total pressure at station 2 was measured by a rake of total-pressure tubes. The weight flow was calculated from the total- and static-pressure readings at station 2 and a correction factor was applied to bring the data in agreement with the theoretical values of supercritical mass flow. The additive drag was then calculated by taking a momentum balance around the surface I, II, III, IV, V, VI, I of figure 4.

## COMPARISON OF THEORY AND EXPERIMENT

### OPEN-NOSE INLETS

The equation for the additive-drag coefficient  $C_{d,a}$  for an open-nose inlet based on the inlet lip area may be derived from equation (5a) as shown in the appendix to give

$$C_{d,a} = \frac{2}{\gamma M_0^2} \left[ \frac{P_0 P_1 p_1}{p_0 P_0 P_1} (\gamma M_1^2 + 1) - 1 - \frac{A_0}{A_1} \gamma M_0^2 \right] \quad (6)$$

where

$$\frac{A_0}{A_1} = \frac{\rho_0 V_0 A_0}{\rho_0 V_0 A_1} = \frac{m}{m_{max}}$$

For given values of  $M_0$  and mass-flow ratio, the value of  $M_1$  can be obtained by applying the continuity equation between stations 0 and 1. This relation may be written in the form

$$\frac{A_0}{A_1} f(M_0) = f(M_1) \frac{P_1}{P_0} \quad (7)$$

where

$$f(M) = M \left( 1 + \frac{\gamma-1}{2} M^2 \right)^{-\frac{\gamma+1}{2(\gamma-1)}}$$

with the usual assumption that  $T_1 = T_0$ . The pressure ratio  $P_1/P_0$  is taken equal to the value across a normal shock occurring at  $M_0$ . Inasmuch as  $p_1/P_1$  and  $p_0/P_0$  are known functions of  $M_1$  and  $M_0$ , all the quantities in equation (6) are determined.

The values of additive-drag coefficient for an open-nose inlet operating at Mach numbers from 1.2 to  $\infty$  have been calculated by the foregoing procedure and are presented in figure 5. For a fixed value of mass-flow ratio  $m/m_{max}$ , the value of  $C_{d,a}$  increases with increasing  $M_0$  and approaches a finite limit for  $M_0 = \infty$ .

A comparison of theoretical (predicted by eq. (6)) and experimental values of additive drag at  $M_0 = 1.8$  and 1.6 (fig. 6) indicates good agreement down to  $m/m_{max} \approx 0.4$ , the

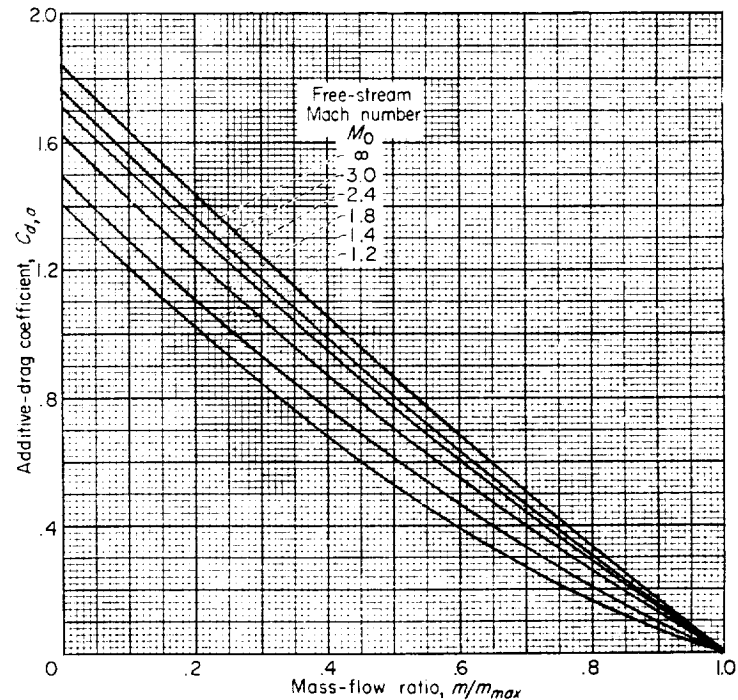


FIGURE 5.—Variation of theoretical additive drag of open-nose inlet with free-stream Mach number.

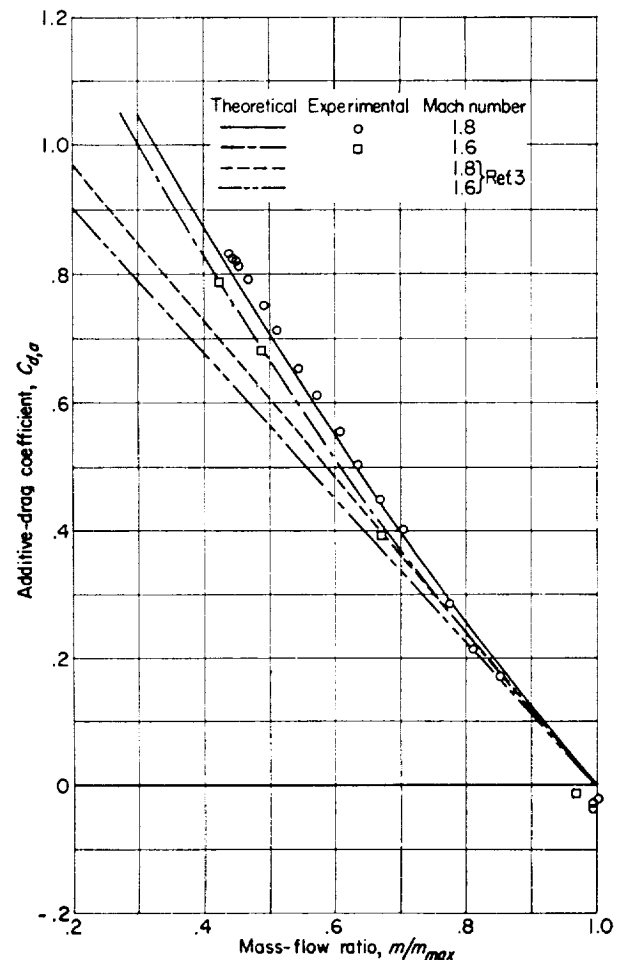
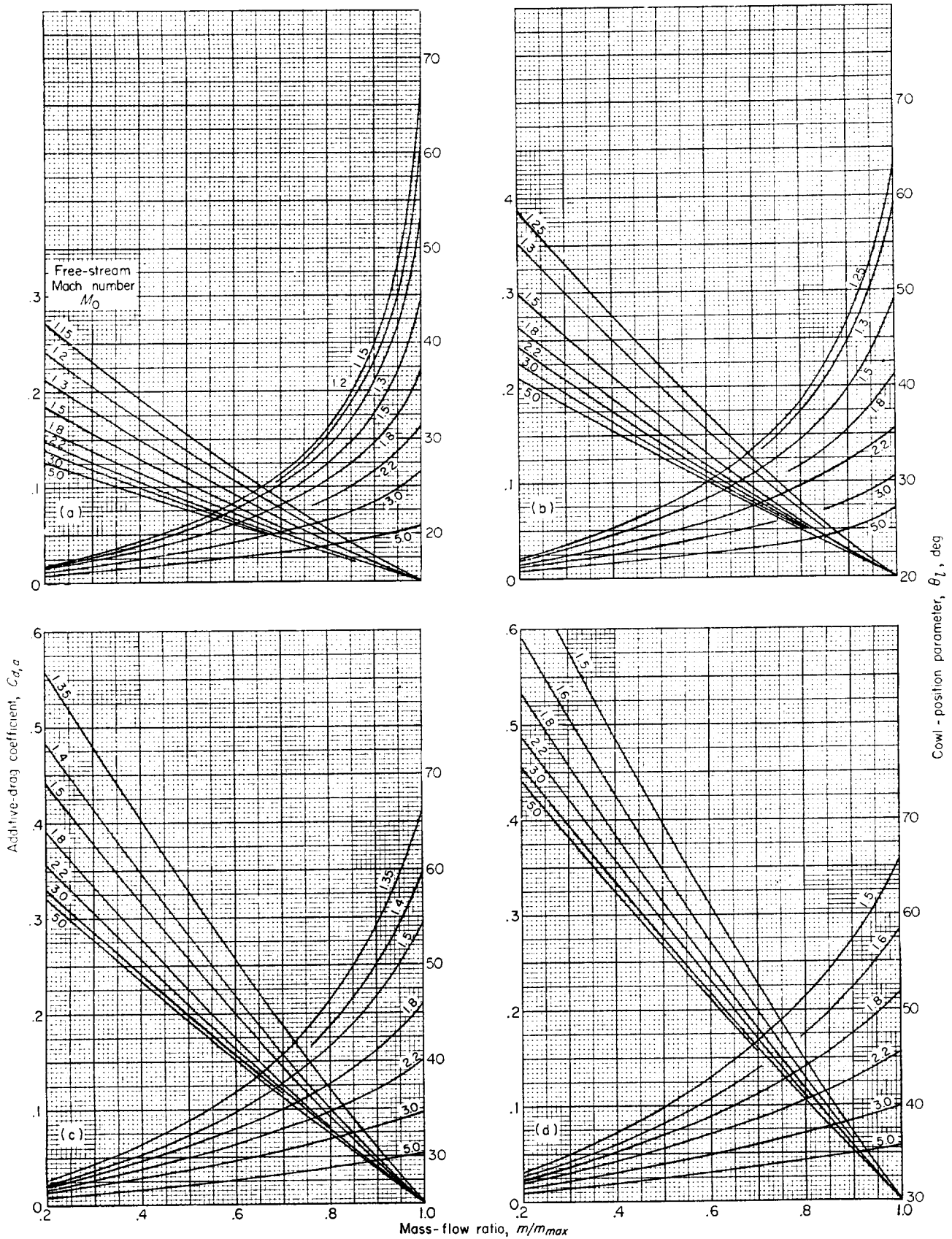


FIGURE 6.—Comparison of experimental and theoretical values of additive drag of open-nose inlet.

lowest mass-flow ratio investigated. Because the additive drag of an open-nose inlet at a mass-flow ratio of 1.0 must equal zero, the discrepancies at that point can be attributed



(a) Cone half-angle, 15°. (b) Cone half-angle, 20°.  
 (c) Cone half-angle, 25°. (d) Cone half-angle, 30°

FIGURE 7.—Variation of theoretical additive drag of annular-nose inlet with conical flow at inlet.

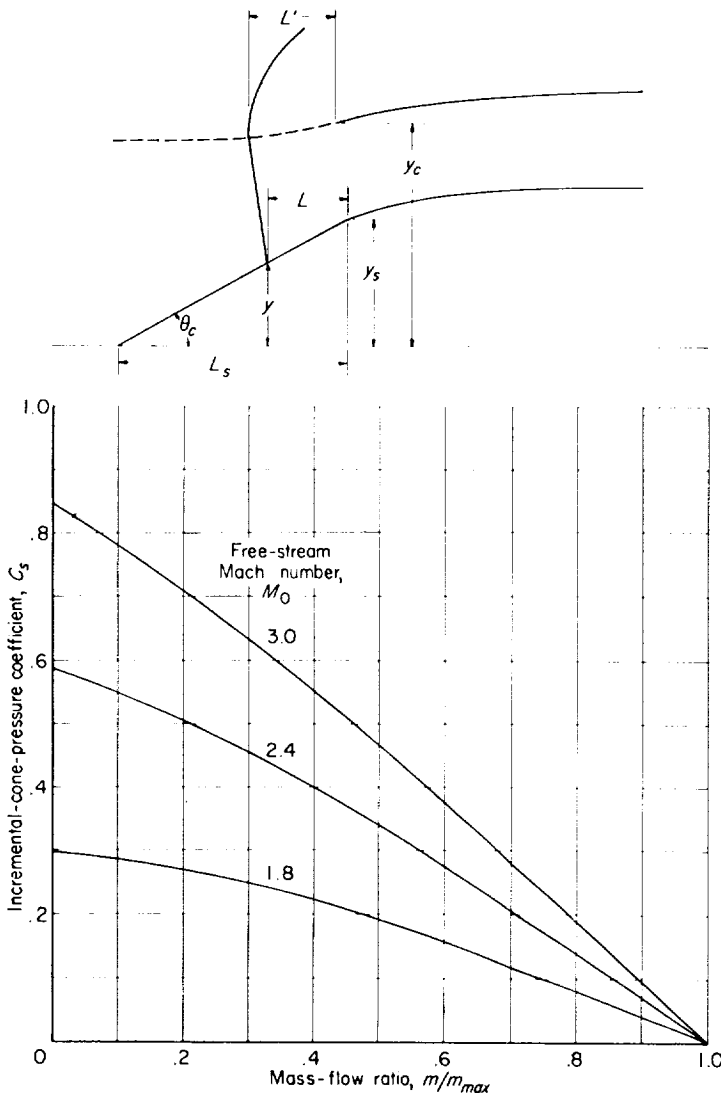


FIGURE 8.—Variation of incremental-cone-pressure coefficient with free-stream Mach number. Cone half-angle,  $25^\circ$ .

to errors in the experimental analysis. Part of this discrepancy is caused by the omission of the unknown force resulting from friction on the inside of the cowl forward of station 2 in calculating the experimental values of additive-drag coefficient. Curves of the additive-drag coefficient predicted by the theory of reference 3 are also shown. This theory predicts a linear variation of additive drag with mass-flow ratio that agrees with the present analysis at mass-flow ratios near 1.0, but underestimates the additive drag at lower mass-flow ratios.

#### ANNULAR-NOSE INLETS

Before discussing additive drag of annular-nose inlets, a basic difference between annular- and open-nose inlets should be considered. When an open-nose inlet is operating without a bow wave, the mass-flow ratio  $m/m_{max}$  must equal 1.0 and, consequently, the additive drag must equal zero. For an annular-nose inlet, however, the mass-flow ratio as herein defined will not equal 1.0 even when no bow wave is present unless the oblique shock stands at or inside the cowl lip. If the oblique shock stands upstream of the cowl lip, it follows that, because of the change in area of the entering stream tube behind the oblique shock, the mass-flow ratio is less

than 1.0 and the additive drag is greater than zero. Consequently, it is useful to define an annular-inlet parameter  $\beta$  equal to the ratio of mass-flow rate with supersonic flow at the inlet to the maximum theoretical capture-area mass flow. For most cases this definition is equivalent to defining  $\beta$  as the supercritical mass-flow ratio. Because from its definition the parameter  $\beta$  is a function only of  $M_0$  and of the geometry of the inlet, an inlet having a value of  $\beta=1.0$  at the design  $M_0$  has a value of  $\beta<1.0$  at an  $M_0$  below design.

**Operation with conical flow at inlet.**—When an annular-nose inlet having a centerbody that is conical forward of station 1 (fig. 3(a)) is operating without any bow waves, the flow behind the oblique shock generated by the centerbody can be predicted from conical flow theory (for example, ref. 5). In this case it is possible to evaluate the additive drag directly from  $\int_1^{\Pi} (p-p_0)dA_r$ . This procedure has been followed for four cone angles over a range of Mach numbers from a value slightly greater than the minimum for an attached shock to an  $M_0$  of 5.0 (fig. 7). The curves show that for a fixed value of mass-flow ratio, the additive-drag coefficient decreases as  $M_0$  increases, which is opposite to the trend in figure 5 for an open-nose inlet. The variation of values of mass-flow ratio with cowl-position parameter  $\theta_i$  is also given from which the theoretical supercritical mass-flow ratio  $\beta$  can be determined when the geometry of the inlet and  $M_0$  are known.

**Operation with bow wave.**—The equation for the additive-drag coefficient based on the capture area  $A_c$  of an annular-nose inlet can be derived from equation (5b) (as shown in the appendix, eq. (A6)) to give

$$C_{d,a} = \frac{2}{\gamma M_0^2} \left[ \frac{A_1 P_0 P_1 p_1}{A_c p_0 P_0 P_1} (\gamma M_1^2 + 1) \cos \lambda + \frac{A_s \bar{p}_s}{A_c p_0} - 1 - \frac{A_0}{A_c} \gamma M_0^2 \right] + C_{f,s} \quad (8)$$

where appropriate average values are used at station 1.

In evaluating equation (8),  $M_1$  can be found by applying the continuity equation (eq. (7)) as a function of  $A_0/A_c = (A_0/A_1)(A_1/A_c)$  if the average pressure recovery  $P_1/P_0$  and flow angle  $\lambda$  are known. For calculations involving an inlet having a centerbody that is conical forward of station 1 when the oblique shock stands at the lip ( $\beta=1.0$ ), the pressure recovery  $P_1/P_0$  is closely approximated by the product of the pressure ratio across an oblique shock and the ratio across a normal shock occurring at the average of the Mach numbers on the cone surface and directly behind the oblique shock. If it is assumed that the average flow angle  $\lambda$  is independent of  $\beta$ ,  $\lambda$  can be determined for an inlet whose  $\beta$  equals 1.0 by the condition that  $C_{d,a}=0$  for  $m/m_{max}=1.0$ . The effect of friction on the centerbody  $C_{f,s}$  is negligible and can be assumed to be zero.

Dailey and McFarland assumed as a first approximation that  $\bar{p}_s/p_0 = p_c/p_0$ . This assumption gives the correct value of additive drag when the mass-flow ratio equals  $\beta$ , and should increasingly underestimate the additive drag as the mass-flow ratio is reduced. It was also assumed that for subcritical flow the value of pressure recovery was constant at the value previously described for  $\beta=1.0$ . An improved approxima-

tion for  $\bar{p}_s/p_0$  and the effect of variations in the pressure recovery from the value assumed are discussed in the following sections.

**Prediction of pressures on centerbody.**—A better approximation for  $\bar{p}_s/p_0$  can be based upon a simplification of the results given in reference 3 for determining the position of a bow wave. In terms of the notation given on the sketch in figure 8, calculations based upon equations in reference 3 show that for an annular-nose inlet with  $\beta \approx 1.0$ , the variation of  $L/y_c$  with mass-flow ratio is approximately linear for  $M_0 \geq 1.6$ . The length  $y_c$  is the radius of the inlet at the cowl lip, and the assumption is made that  $L=L'$ , where  $L$  is the axial distance from the point where  $A_s$  is measured to the point where the bow wave intersects the centerbody. As a simplification it will be assumed that  $L/y_c = K(1 - m/m_{max})$ ;  $K$  is independent of cone angle and its variation with  $M_0$  is given in the following table:

$M_0$	1.6	2.0	2.4	2.8	3.2
$K$	1.13	.89	.76	.69	.65

The values of  $K$  were determined by plotting  $L/y_c$  against mass-flow ratio and finding the mean slope of the curves. Then, from the geometry of the figure,

$$y = y_s - y_c K (1 - m/m_{max}) \tan \theta_c$$

where  $y_s$  is the radius at  $A_s$ . This gives

$$\frac{A_v}{A_c} = \left[ \sqrt{\frac{A_s}{A_c}} - K(1 - m/m_{max}) \tan \theta_c \right]^2 \quad (9)$$

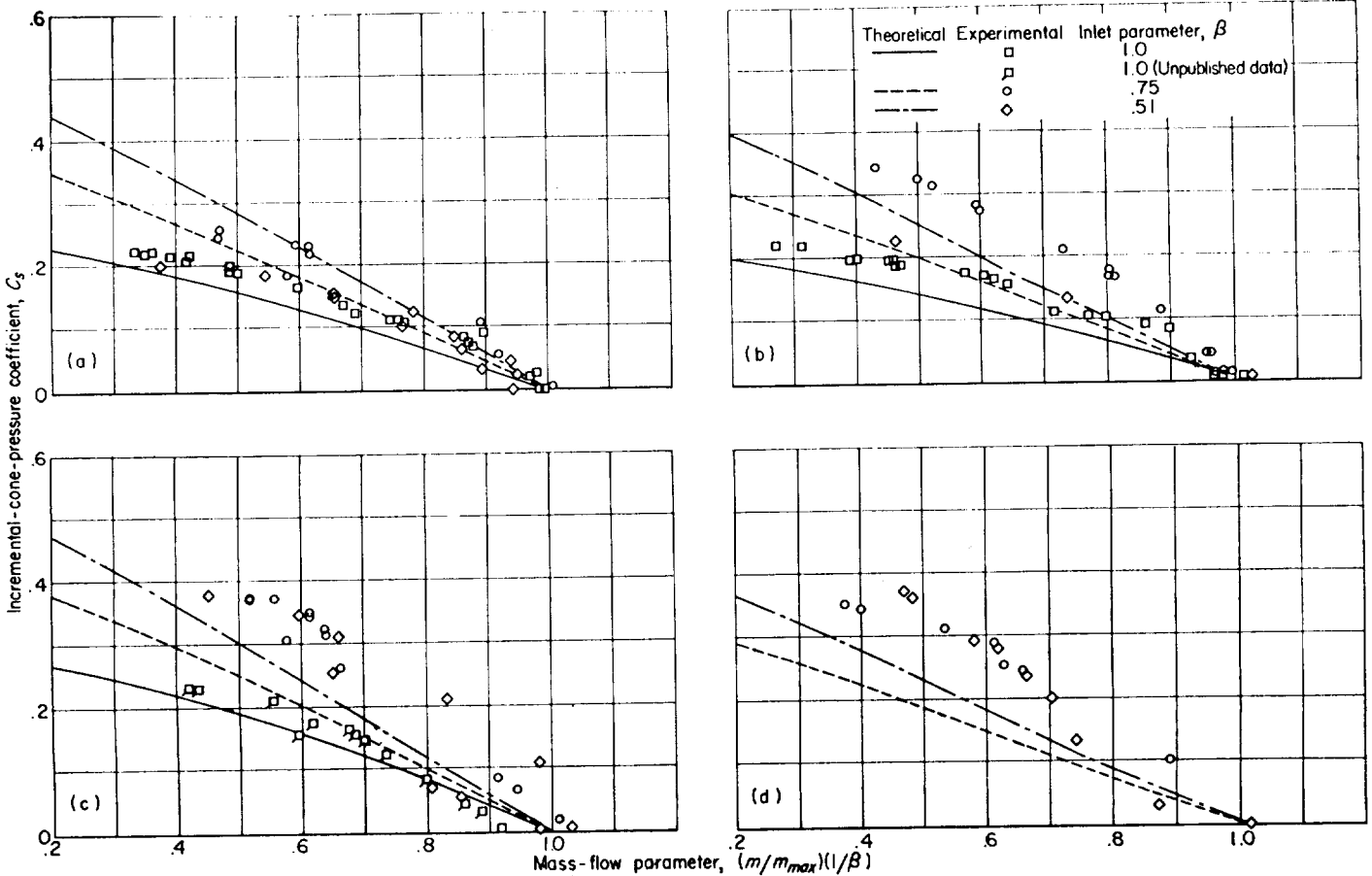
from which  $A_v$  can be calculated.

Forward of  $A_v$ , the pressure on the centerbody equals the previously assumed value of  $p_c$ . The average pressure  $\bar{p}$  behind  $A_v$  will lie between  $p_1$  and the static pressure behind a normal shock at the cone surface Mach number  $p_y$ . It will be assumed that  $\bar{p} = (p_y + p_1)/2$ . An incremental-cone-pressure coefficient  $C'_s \equiv 2A_s(\bar{p}_s - p_c)/\rho_0 V_0^2 A_c$  can now be defined. When added directly to the value of  $C_{d,a}$  obtained using the approximation  $\bar{p}_s = p_c$ ,  $C'_s$  will account for the increase in additive drag caused by the increase of pressure on the cone behind the bow wave. Using the development given yields

$$C'_s = \frac{2}{\gamma M_0^2} \frac{(A_s - A_v)(\bar{p} - p_c)}{A_c p_0} \quad (10)$$

The variation of  $C'_s$  with mass-flow ratio for a 25° half-angle cone is shown in figure 8 for a range of  $M_0$ .

Although the approximate relation  $L/y_c = K(1 - m/m_{max})$  is based upon a derivation in reference 3 for inlets with  $\beta \approx 1$ , it will be assumed that for other inlets the relation  $L/y_c = K[1 - (m/m_{max})(1/\beta)]$  is approximately true, where the



(a) Cone half-angle, 20°; Mach number, 1.8.  
 (c) Cone half-angle, 25°; Mach number, 1.8.

(b) Cone half-angle, 20°; Mach number, 1.6.  
 (d) Cone half-angle, 25°; Mach number, 1.6.

FIGURE 9.—Comparison of theoretical and experimental values of incremental-cone-pressure coefficient.

values of  $K$  are the same as those given previously. With this approximation, a comparison of the variation of the theoretical and experimental values of  $C'_s$  with  $(m/m_{max})(1/\beta)$  is shown in figure 9. For a given  $M_0$  at a fixed value of  $(m/m_{max})(1/\beta)$ , the theory predicts that  $C'_s$  increases as  $\beta$  decreases. The scatter of the experimental data is, however, too great to allow a conclusion to be drawn as to the variation of  $C'_s$  with  $\beta$  for the inlets tested. For mass-flow ratios less than approximately 0.85 to 0.95, the flow into the inlets was pulsating so that the model upon which the theoretical results are based can only be considered to represent an average condition and scatter in the data is to be expected. Nevertheless, for  $\theta_c=20^\circ$ , the theory agrees with the data

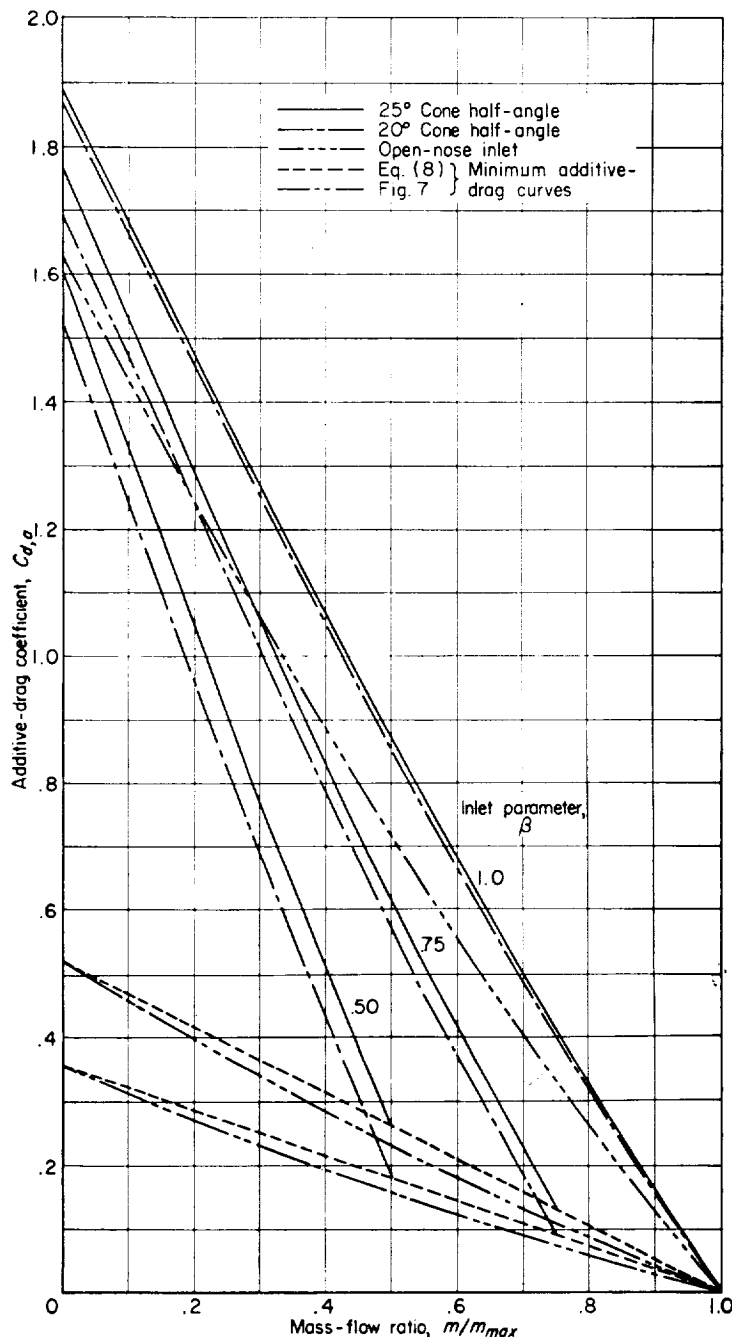


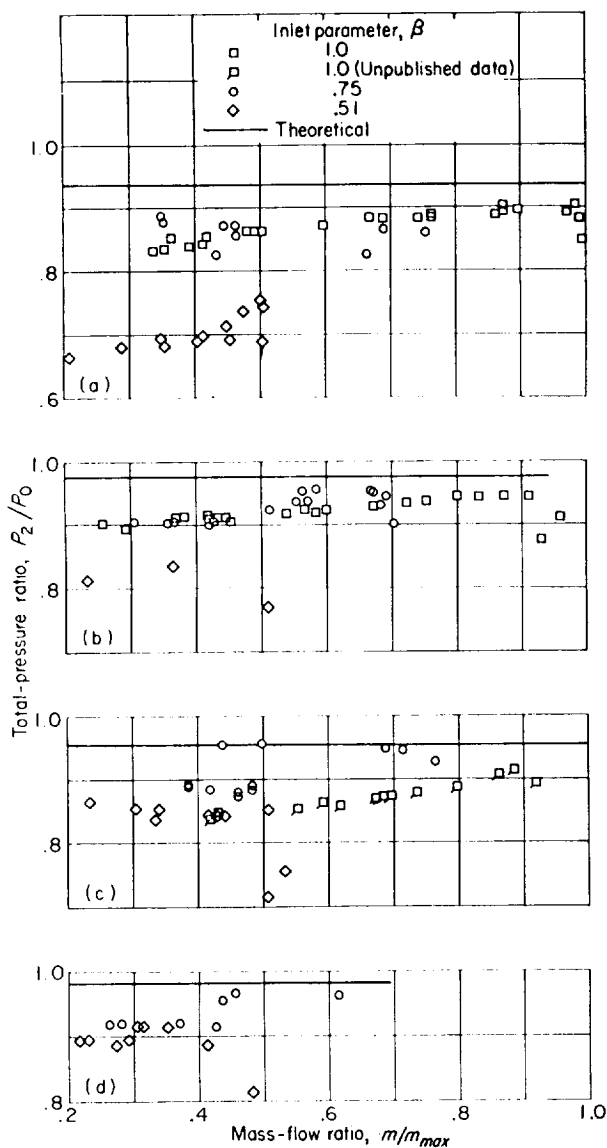
FIGURE 10.—Effect of cone angle and inlet parameter  $\beta$  on additive drag. Mach number, 1.8.

moderately well; for  $\theta_c=25^\circ$ , the experimental values are greater than theoretical. In all cases the theory is an improvement over the previous assumption, which corresponds to  $C'_s=0$ .

The variation of additive-drag coefficient with mass-flow ratio as calculated from equation (8) including the effect of the incremental-cone-pressure coefficient  $C'_s$  and using the value of pressure recovery  $P_1/P_0$ , described previously for  $\beta=1.0$ , is shown in figure 10 at three values of  $\beta$  for each of two annular inlets operating at  $M_0=1.8$ . For comparison, the value of additive-drag coefficient for an open-nose inlet at the same  $M_0$  is also shown. For a fixed value of mass-flow ratio and as  $\beta$  decreases from 1.0, the additive drag decreases from a value greater than that for an open-nose inlet to a minimum when the flow at the inlet is supersonic. Curves of the minimum value of  $C'_{d,a}$ , as determined from equation (8) which is obtainable at each value of mass-flow ratio (that is, when the flow at the inlet is supersonic), are also shown for both cone angles. Comparable curves computed from conical flow theory (fig. 7) are shown for comparison. The differences in these minimum additive-drag curves can be attributed to the small changes in pressure recovery and flow angle  $\lambda$  that occur as  $\beta$  is reduced and which were neglected in the evaluation of equation (8). Each point on these minimum  $C'_{d,a}$  curves corresponds to a different inlet configuration, whereas the curves for a given  $\beta$  refer to one inlet. From figure 10, if a given amount of air must be spilled it is better, from additive-drag considerations, to achieve this by allowing the oblique shock to stand upstream of the cowl lip rather than by spilling the air behind a bow wave. Consequently, for an engine designed to operate over a range of  $M_0$ , an appreciable gain in net propulsive thrust can be realized at values of  $M_0$  below the design value by utilizing an inlet in which the projection of the centerbody increases as  $M_0$  decreases to maintain supersonic flow at the inlet.

**Effect of inlet total-pressure recovery.**—The additive-drag curves of figure 10 assume that the pressure recovery  $P_1/P_0$  is constant at the value calculated for  $\beta=1.0$ . The experimental total-pressure ratio between stations 0 and 2 is shown in figure 11 and compared with the assumed value of  $P_1/P_0$ . If it is assumed that  $P_2/P_1$  is very close to 1.0, the difference between the experimental and theoretical values indicates that the effect on additive drag of a reduction in pressure recovery should be considered. The effect on additive drag of varying the ratio of assumed pressure recovery to the recovery for  $\beta=1.0$  from 1.0 to 0.8 at two values of  $\beta$  for an annular inlet with a  $20^\circ$  half-angle cone at  $M_0=1.8$  is shown in figure 12. Overestimating the pressure recovery overestimates the additive drag by an amount that is independent of mass-flow ratio for a given value of  $\beta$  but decreases as  $\beta$  decreases.

Experimental values of additive drag obtained from tests of annular-nose inlets are shown in figure 13 for free-stream Mach numbers of 1.8 and 1.6. These results are compared with the theoretical curves obtained from equation (8) using the approximations of Dailey and McFarland. Comparison is also made with theoretical curves using the approximation for  $\bar{p}_s/p_0$  presented in this paper and experimental values of



(a) Cone half-angle, 20°; free-stream Mach number, 1.8.  
 (b) Cone half-angle, 20°; free-stream Mach number, 1.6.  
 (c) Cone half-angle, 25°; free-stream Mach number, 1.8.  
 (d) Cone half-angle, 25°; free-stream Mach number, 1.6.

FIGURE 11.—Comparison of theoretical and experimental values of inlet total-pressure recovery.

pressure recovery. The curves calculated with the present method also begin at the more exact values of additive-drag coefficient given in figure 7.

The discrepancies between the experimental data and the theoretical curves of the present method at and near supercritical flow conditions can be attributed primarily to the omission of the unknown force due to friction on the centerbody and cowl forward of station 2 in calculating the experimental values of additive-drag coefficient. This error is greatest near supercritical flow conditions and decreases as the mass-flow ratio decreases. At lower values of mass-flow ratio, the differences between theory and experiment are due primarily to the error made in predicting the magnitude of the force resulting from the variable static pressures on the centerbody, as can be seen by comparing the differences

between theory and experiment in figures 9 and 13. As previously suggested, these errors may be due in part to the pulsating condition of the flow at low mass-flow ratios.

The good agreement shown here between the experimental data for inlets with  $\beta=1$  and the theoretical curves obtained using the assumptions of Dailey and McFarland is due to a fortuitous cancellation of the errors due to assuming higher pressure recoveries and lower pressures on the centerbody than those actually obtained.

#### CALCULATION OF ADDITIVE DRAG FROM SCHLIEREN PHOTOGRAPHS

Another means of calculating additive drag, which approaches the problem from a different viewpoint, can be obtained from the method suggested by Nucci. This method allows the sum of the additive and cowl-pressure drags to be computed using a schlieren photograph of the inlet shock configuration and knowing the mass-flow ratio  $m/m_{max}$ . If the cowl-pressure drag can be determined by another method, subtracting it from the sum of the two drags will give the additive drag. The method involves taking a momentum balance around the surface, I, II, III, III', IV, V, VI, I as shown in figure 14, where it is assumed that the cowl is cylindrically extended downstream from its point of maximum diameter III, to station X so that  $p_X \equiv p_0$  and  $A_{III'} \equiv A_{III}$ . An arbitrary point V on the bow wave is then chosen and the streamline VI, V, IV extended through it. Then

$$\int_{II}^{III} (p-p_0)dA_x = m(V_0 - V_X) + (\bar{p}_{IV,V} - p_0)(A_{IV} - A_V) \quad (11)$$

where  $\int_{II}^{III} (p-p_0)dA_x$  defines the sum of the additive and cowl-pressure drags. Two alternative assumptions have been suggested for  $\bar{p}_{IV,V}$ ; namely,  $\bar{p}_{IV,V} = p_w$  at V, which gives an upper limit, and  $\bar{p}_{IV,V} = (p_w + p_0)/2$ , which generally gives a lower limit. The flow is also assumed to be isentropic behind the bow wave.

In order to evaluate equation (11), it is necessary to determine  $m$ ,  $V_X$  (or  $M_X$ ), and  $A_{IV}$ . The mass flow  $m$  can be calculated from  $\rho_0 V_0 (A_{VI} - A_I)$ , where  $A_I$  is a function of the given mass-flow ratio. The total pressure behind the bow wave  $\bar{P}_{II,V}$  can be determined by properly weighting the total-pressure loss across the bow wave at several points from II to V. Then from the isentropic flow assumption,  $M_X$  can be determined from  $p_0/\bar{P}_{II,V}$ . Finally,  $A_{IV}$  can be computed by applying the continuity equation between stations 0 and X.

The results of such a calculation for additive-drag coefficient, using a shock length of two inlet diameters, are shown in figure 14 for an annular inlet with a 25° half-angle cone operating at  $M_0=1.79$  and compared with values obtained from unpublished pressure measurements.

The curves show that for the shock length used the assumption made for  $\bar{p}_{IV,V}$  greatly influences the results. For the engine tested, the assumption that  $\bar{p}_{IV,V} = (p_w + p_0)/2$  gave good agreement, especially at high mass-flow ratios. In order to determine the importance of accurately determining the average pressure ratio across the portion of the bow wave

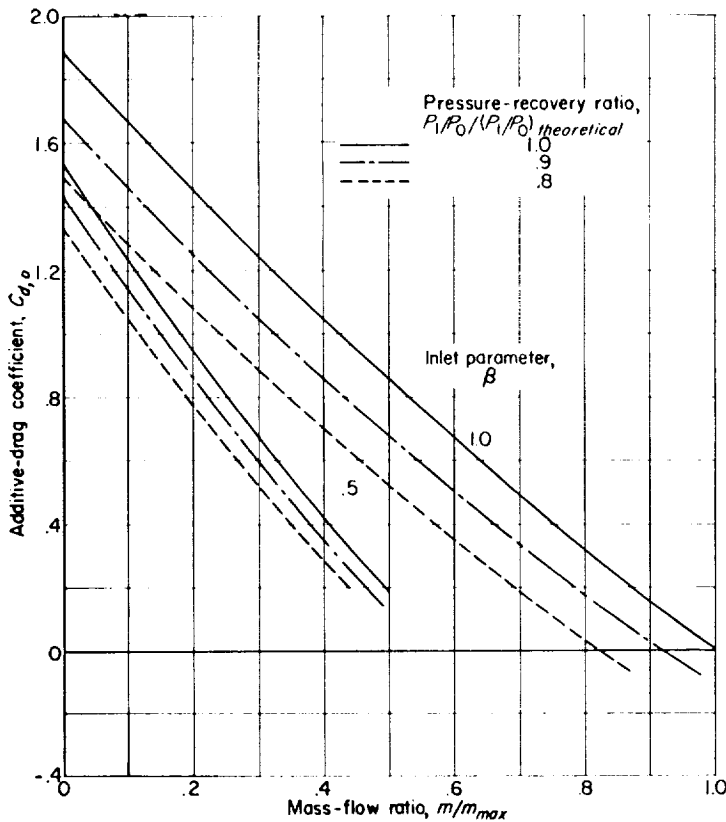


FIGURE 12.—Effect of inlet total-pressure recovery on additive drag. Cone half-angle,  $20^\circ$ ; Mach number, 1.8.

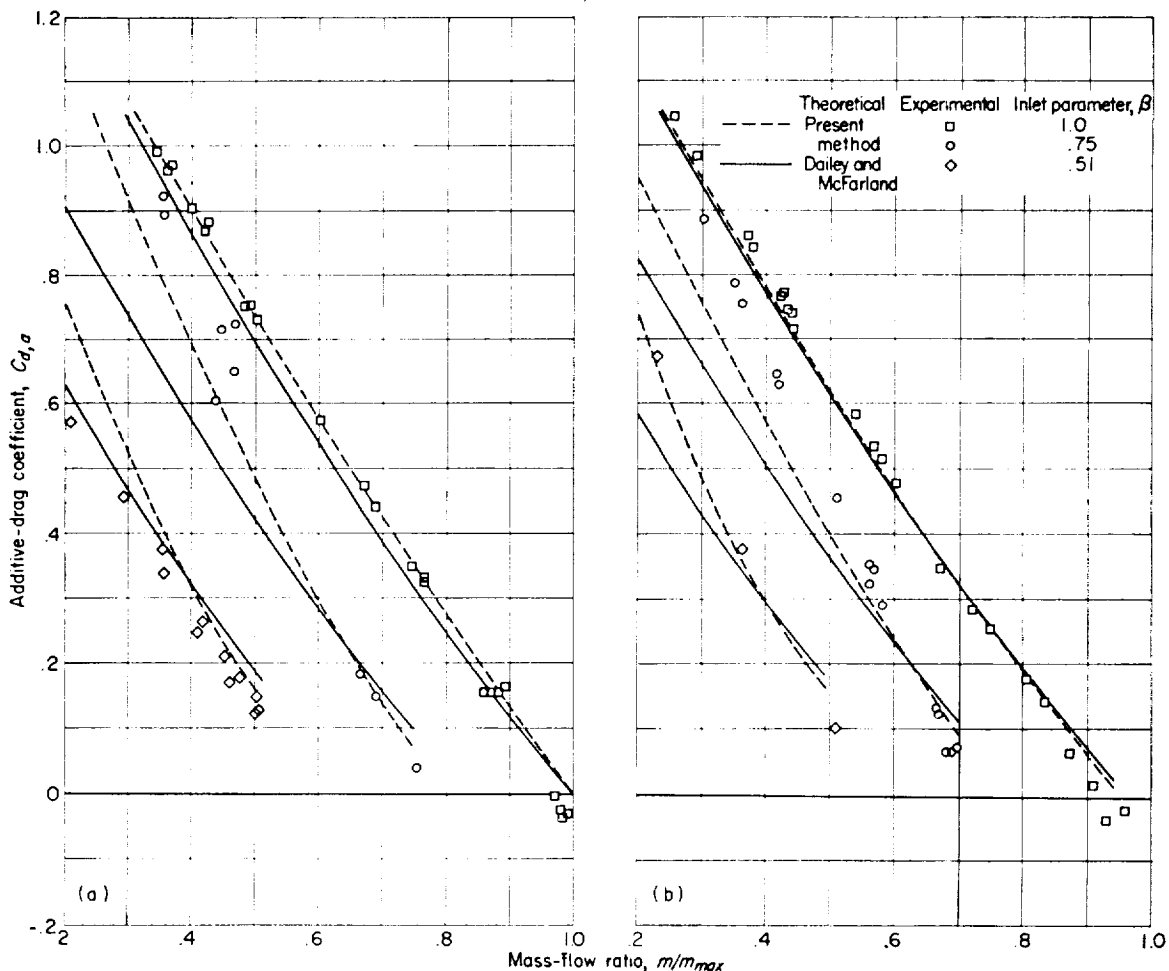
considered, the effect on the values of additive drag of an error of 0.5 percent in  $\bar{P}_{11,v}$  was also calculated (by multiplying the computed  $\bar{P}_{11,v}$  by 0.995) and is shown for each assumption of  $\bar{p}/v,v$ ; the effect is relatively small.

SUMMARY OF RESULTS

Formulas were developed for determining the additive drag of annular- and open-nose inlets. Calculations based upon these formulas showed that for a fixed lip area and cone angle the additive drag at a given mass-flow ratio varied with the projection of the centerbody and was least when the flow at the inlet was supersonic.

The effect on additive drag of changes in the free-stream Mach number was relatively small. For annular inlets, the additive drag decreased with increasing Mach number when the flow at the inlet was supersonic but increased with increasing Mach number for most cases when there was a bow wave ahead of the inlet. For open-nose inlets, the additive drag increased with increasing Mach number.

The forces due to the variation of static pressure on the centerbody with mass-flow ratio were considered, and an analytical method of approximating their value was developed which showed that they represented an appreciable portion of the additive drag. Overestimating the inlet total-pressure recovery resulted in an estimate of additive drag that was too large.



(a) Cone half-angle,  $20^\circ$ ; Mach number, 1.8. (b) Cone half-angle,  $20^\circ$ ; Mach number, 1.6.

FIGURE 13.—Comparison of theoretical and experimental variations of additive drag with mass-flow ratio for several centerbody projections.

Comparisons of the theoretical values of additive drag with experimental results showed excellent agreement for an open-nose inlet and moderate agreement for several annular-nose inlets when the effects of variable centerbody pressures and inlet pressure recovery were considered in obtaining the theoretical results.

Consideration of a proposed method of obtaining the external drag from schlieren photographs showed that when a shock length of two inlet diameters was used the results

depended largely upon the value of one of the assumptions involved. For the particular configuration to which this method was applied, one of the suggested values for this assumption gave good agreement with the value of additive drag obtained from pressure measurements.

LEWIS FLIGHT PROPULSION LABORATORY  
 NATIONAL ADVISORY COMMITTEE FOR AERONAUTICS  
 CLEVELAND, OHIO, February 1, 1951.

APPENDIX

DERIVATION OF ADDITIVE-DRAG COEFFICIENT  $C_{d,a}$  FOR ANNULAR- AND OPEN-NOSE INLETS

The additive drag for an annular inlet is given in the text (eq. (5b)) as

$$D_a = mV_1 \cos \lambda + A_1 \cos \lambda (p_1 - p_0) + A_s (\bar{p}_s - p_0) - mV_0 + F_{f,s} \tag{A1}$$

but it can be seen from figure 3 (a) that

$$A_c = A_1 \cos \lambda + A_s$$

then

$$D_a = mV_1 \cos \lambda + A_1 p_1 \cos \lambda + A_s \bar{p}_s - A_c p_0 - mV_0 + F_{f,s} \tag{A2}$$

Substituting

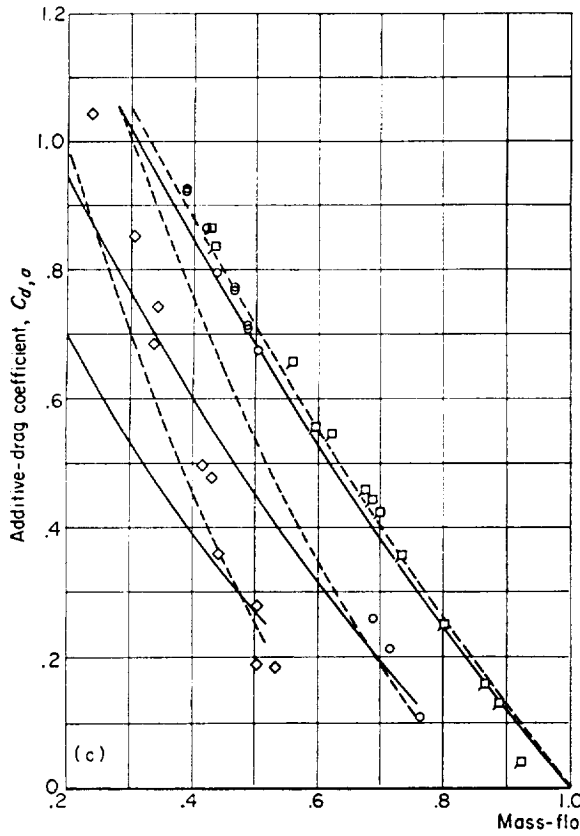
$$m = \rho AV \text{ and } \rho = p/gRt$$

gives

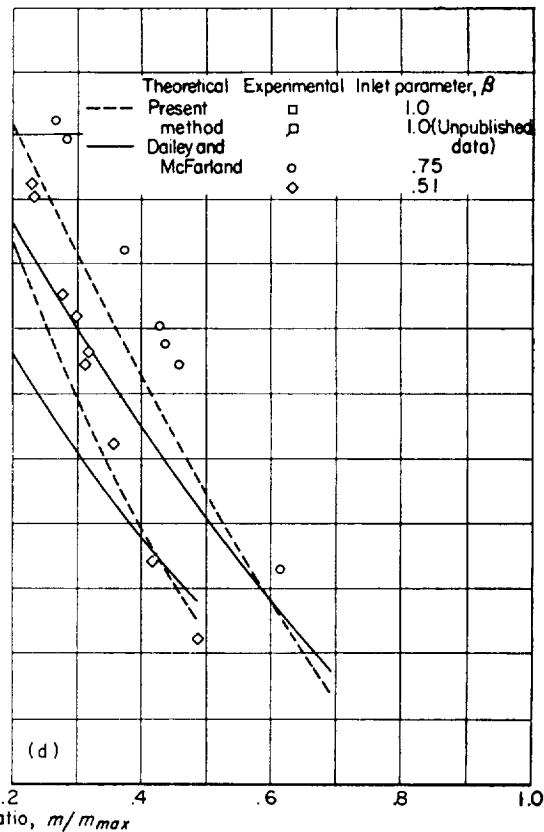
$$D_a = \frac{p_1 A_1 V_1^2 \cos \lambda \gamma}{gRt_1} + A_1 p_1 \cos \lambda + A_s \bar{p}_s - A_c p_0 - \frac{p_0 A_0 V_0^2 \gamma}{gRt_0} + F_{f,s} \tag{A3}$$

Substituting  $M^2 = V^2/\gamma gRt$  and dividing by  $A_c p_0$  gives

$$\frac{D_a}{A_c p_0} = \frac{A_1 p_1 \gamma M_1^2 \cos \lambda}{A_c p_0} + \frac{A_1 p_1 \cos \lambda}{A_c p_0} + \frac{A_s \bar{p}_s}{A_c p_0} - 1 - \frac{A_0 \gamma M_0^2}{A_c} + \frac{F_{f,s}}{A_c p_0} \tag{A4}$$



(c) Cone half-angle, 25°; Mach number, 1.8.



(d) Cone half-angle, 25°; Mach number, 1.6.

FIGURE 13.—Concluded. Comparison of theoretical and experimental variations of additive drag with mass-flow ratio for several centerbody projections.

Substituting  $\frac{p_1}{p_0} = \frac{P_0 P_1 p_1}{p_0 P_0 P_1}$ , rearranging, and converting into coefficient form gives

$$C_{d,a} = \frac{2}{\gamma M_0^2} \left[ \frac{A_1 P_0 P_1 p_1}{A_c p_0 P_0 P_1} (\gamma M_1^2 + 1) \cos \lambda + \frac{A_s \bar{p}_s}{A_c p_0} - 1 - \frac{A_0}{A_c} \gamma M_0^2 \right] + C_{f,s} \quad (A5)$$

The value of  $C_{d,a}$  for an open-nose inlet can be derived from equation (A5) by noting that for an open-nose inlet  $A_1 = A_c$ ,  $\cos \lambda = 1$ ,  $A_s = 0$ , and  $C_{f,s} = 0$ , which reduces equation (A5) to (eq. (6) of the text)

$$C_{d,a} = \frac{2}{\gamma M_0^2} \left[ \frac{P_0 P_1 p_1}{p_0 P_0 P_1} (\gamma M_1^2 + 1) - 1 - \frac{A_0}{A_1} \gamma M_0^2 \right] \quad (A6)$$

REFERENCES

1. Ferri, Antonio, and Nucci, Louis M.: Preliminary Investigation of a New Type of Supersonic Inlet. NACA Rep. 1104, 1952. (Supersedes NACA TN 2286.)
2. Fradenburgh, Evan A., and Wyatt, DeMarquis D.: Theoretical Performance Characteristics of Sharp-Lip Inlets at Subsonic Speeds. NACA TN 3004, 1953.
3. Moeckel, W. E.: Approximate Method for Predicting Form and Location of Detached Shock Waves Ahead of Plane or Axially Symmetric Bodies. NACA TN 1921, 1949.
4. Klein, Harold: The Calculation of the Scoop Drag for a General Configuration in a Supersonic Stream. Rep. No. SM-13744, Douglas Aircraft Co., Inc., Apr. 12, 1950.
5. Anon.: Tables of Supersonic Flow Around Cones. Vol. 1. Dept. Elec. Eng., M. I. T., 1947.

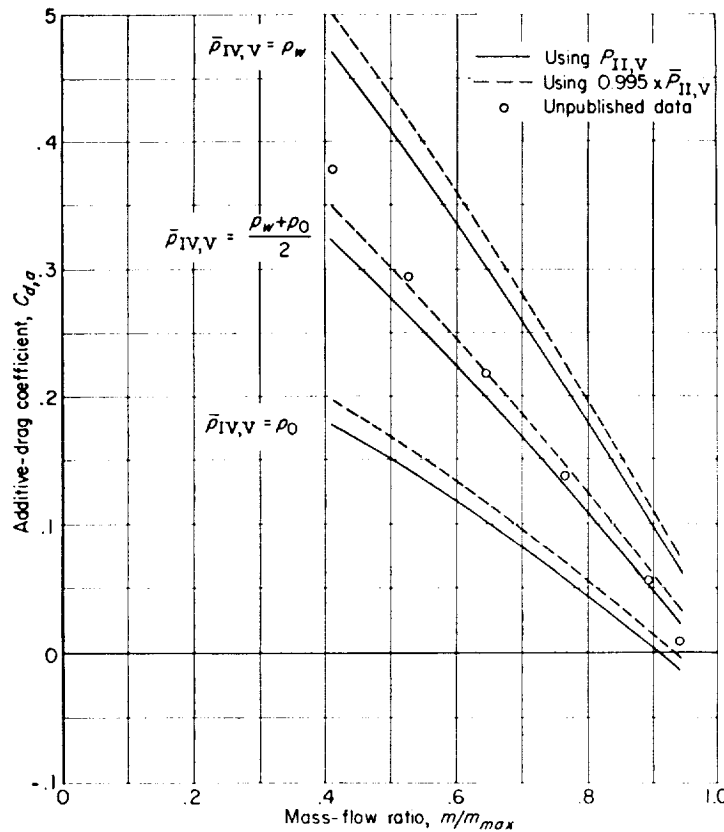
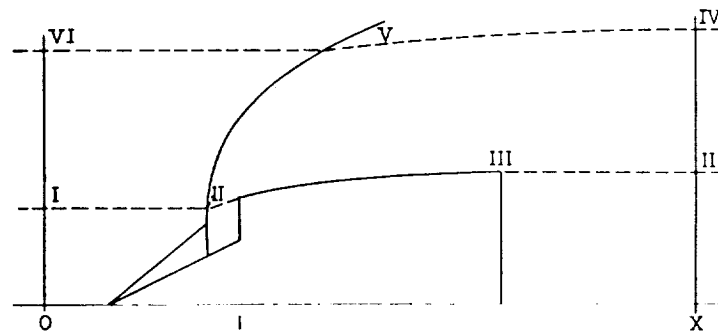


FIGURE 14.—Comparison of values of additive drag obtained from schlieren photographs and from pressure measurements. Mach number, 1.79.



